# A Study on the Pressure Loss, Heat Transfer Enhancement and Fouling Control in a Vertical Particulate Flow

**Nae-Hyun Kim*, Youn-Pyo Lee**, Seong-Young Youn** and Jong-Soo Jurng****

*(Received April 3, 1995)*

In this study, the pressure loss, the heat transfer rate and the fouling characteristics of a particulate flow were investigated. Particles used were the glass beads of 3.0 mm diameter with 2.54 specific gravity. The particles augmented the heat transfer at the flow velocities lower than 1.0 m/s. In this range, the heat transfer coefficient slighly increased as the particle volume fraction increased, and was almost independent of the flow velocity. The particles also increased the pressure loss at the flow velocities lower than 1.0 m/s. Above 1.0 m/s, however, the heat transfer coefficient and the pressure loss were essentially the same as those of flow with pure water. Through the flow visualization study, the collision frequency on the wall by particles is shown to be closely related with the heat transfer enhancement. The particles effectively controlled fouling. Fouling tests using ferric oxide revealed that the particles effectively removed the pre-exsisting deposit as well as they prevented the deposit buildup.

**Key Words:** Particulate Flow, Pressure Loss, Heat Transfer Enhancement, Fouling

**Nomenclatures**

$Ar$ : Archimedes number (Eq.(7))
$c_{ps}$ : Specific heat of the particle (J/kgK)
$c_{pw}$ : Specific heat of water (J/kgK)
$C_d$ : Drag coefficient of a swarm of particles
$C_{do}$ : Drag coefficient of a single particle
$C_v$ : Volume fraction of particles
$d$ : Praticle diameter (m)
$D$ : Tube inside diamter (m)
$F_r$ : Froude number (Eq.(3))
$g$ : Gravity (m/s$^2$)
$h$ : Water column height (m) or heat transfer coefficient (W/m$^2$ K)
$i_f$ : Pressure loss per length for water flow (Pa/m)
$i_m$ : Pressure loss per length for slurry flow (Pa/m)
$I$ : Current (A)
$k$ : Thermal conductivity (W/m K)
$L$ : Length between pressure taps or heat transfer test section (m)
$m_s$ : Mass flow rate of particles (kg/s)
$m_w$ : Mass flow rate of water (kg/s)
$Nu_p$ : Particle Nusselt number ($=hd_p/k$)
$Pr$ : Prandtl number
$Q$ : Heat transferred to the test section (W)
$Re_p$ : Particle Reynolds number (Eq.(6))
$s$ : Specific gravity of a particle
$t$ : Time (sec)
$T_f$ : Average water temperature (K)
$T_{in}$ : Water inlet temperature (K)
$T_o$ : Wall temperature of the glass wool (K)
$T_{out}$ : Water outlet temperature (K)
$T_w$ : Wall temperature (K)
$V$ : Superficial velocity (m/s) or electric voltage (Volt)
$V_w$ : Water velocity (m/s)
$V_p$ : Particle velocity (m/s)
$V_s$ : Slip velocity of a particle ($=V_w-V_p$) (m/s)
$\Delta h_c$ : Correction term for the pressure head (m)
$\Delta h_m$ : Pressure head from the manometer (m)
$\Delta h_p$ : Pressure head (m)
$\phi$ : Pressure loss coefficient (Eq.(8))
$\upsilon$ : Dynamic viscosity [m$^2$/s]

* Department of ME, University of Inchon
** Thermal/Fluids Engineering Lab., Korea Institute of Science and Technology

## 1. Introduction

"Fouling" may be defined as the deposition of unwanted materials on heat transfer surfaces, which increases the pressure loss and degrades the thermal performance of a heat exchanger. Especially when the processing fluid contains foreigh materials, fouling control becomes an important issue. In a certain occasion, the thermal fouling resistance exceeds half of the total thermal resistance. To remove the deposit, a number of techniques have been developed. They include both mechanical and chemical methods. In mechanical methods, sponge balls or brushs are circulated with the fluid, and remove the deposit. In chemical methods, chemicals such as chlorine, acid are added into the fluid to soften the deposit, and the flow eventually removes the deposit. Chemical methods are widely used. However, added chemicals may induce secondary environmental problems. To adopt mechanical methods, additional pumps or valves are necessary.

A fluidized bed heat exchanger with circulating liquid has been used successfully where fouling is a major concern. In United States, it was developed as a brine heater of a desalination plant (Hatch and Weth, 1970). In Netherlands, it was used for the brine heating and heat recovery in multi-stage flash evaporators(Klaren, 1983). In Germany, fluidized bed technique was applied to waste water treatment(Rautenbach et al., 1991). We ourselves became interested in a fluidized bed heat exchanger in connection with a waste water evaporator. Figure 1 shows the sketch of circulating glass beads in our fluidized bed heat exchanger. The fluidized bed heat exchanger consists of a number of ascending tubes and a descending tube. The descending tube is located at the center of the heat exchanger. Glass beads rise through the ascending tubes and return back through the descending tube. A stainless steel check ball located at the bottom of the heat exchanger prevents outflow of beads during system shut-down.

Fluidized bed heat exchangers are known to have a number of merits - it increases the heat transfer and prevents the fouling. To design a fluidized bed heat exchanger, friction and heat transfer characteristics of the slurry flow are needed. In this study, friction and heat transfer tests were conducted in a single vertical tube. Glass beads of 3.0mm diameter(specific gravity of 2.54) were circulated with water. Pressure drop and heat transfer coefficients were measured. By visualizing the particle behavior near tube wall, a possible heat transfer enhancement mecha-

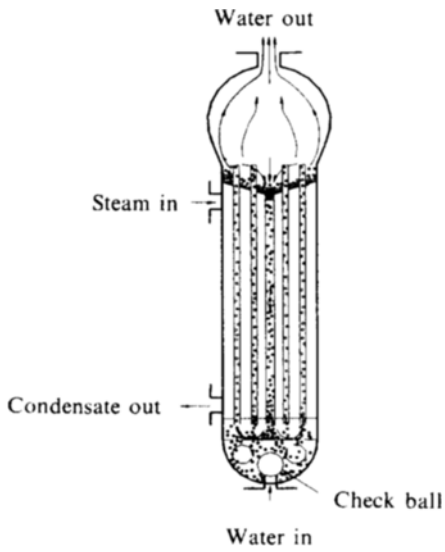


**Fig. 1** Sketch showing circulating glass beads in the fluidized heat exchanger.

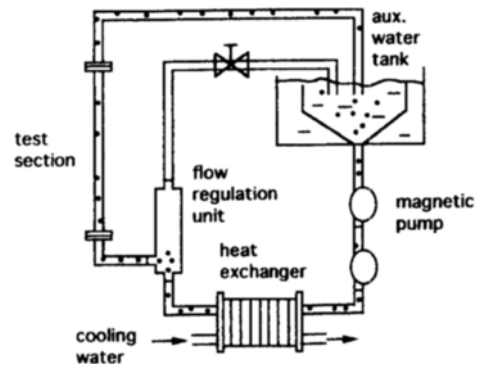


**Fig. 2** Schematic drawing of the experimental apparatus used for the pressure loss and the heat transfer test.

nism was proposed. Fouling tests were also performed using ferric oxide. It is shown that glass beads control the fouling effectively.

## 2. Experimental Apparatus

Two different experimental apparatus were built - one for the pressure loss and the heat transfer tests, the other for the flow visualization test. Figure 2 shows the apparatus used for the pressure loss test. The apparatus consists of a pump, a flow regulation unit, a water tank, a heat exchanger and a test section. Magnetic pump was chosen because the wide impeller spacing of the pump made glass beads pass through easily. Two magnetic pumps of 190 W capacity each were connected in series to provide sufficient flow to the system. Flow rate was controlled by a flow regulation unit which bypasses a relevant amount of water back to the reservoir. At the downstream of the test section, a heat exchanger was installed to remove the heat supplied to the test section.

Except for the flow visualization test, all the tests were conducted at the same flow loop. Test sections were changed accordingly. For the pressure drop and the heat transfer test, test sections were made of copper tube with 14.0 mm inner diameter. They are shown in Fig. 3. For the pressure drop measurement, three pressure taps were machined on a 2m long copper tube. The distance between taps was 370mm. Sufficient entrance length (approximately 1 m) was provided prior to the first pressure tap. Pressure drop was measured using a water manometer.

Heat transfer tests were conducted in a 1.4 m long copper tube. A Ni-Cr heater of 5 mm width was wrapped around the copper tube, and an electric current was supplied to the heater. Thin asbestos tape was wrapped between the heater and the copper tube to provide electric insulation. The test section was then insulated with a glass wool of 5 cm thickness. Tube wall temperatures were measured by thermocouples. Figure 3 also shows the detail of the thermocouple installation. Slits of 20mm length, 1mm width, 0.7mm depth were first machined on the outer surface of the copper tube. Thermocouples were attached in the slits using a small amount of soft solder, and the remaining portion of the slit was filled with silver paste. Six thermocouples were mounted in axial direction at 20cm interval. Teflon coated copper -constantan thermocouples of 0.3 mm diameter were used. Inlet and outlet water temperatures were accurately measured using 5 junction thermopiles. Flow rate was determined by weighing the circulating water. To minimize the system variation during flow measurement, fresh water from the auxiliary water tank was continuously added to the system.

Figure 4 shows the schematic diagram of the experimental setup for flow visualization test. The test section consists of a glass tube with 12mm inner diameter and 700mm length. Flow was

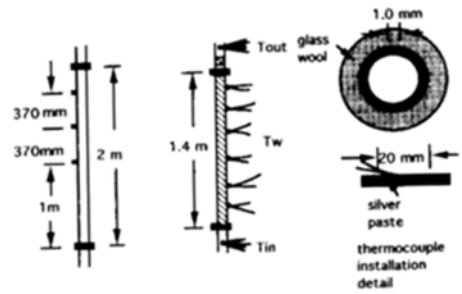


(a) Test section for pressure drop test (b) Test section for heat transfer test

**Fig. 3** Schematic details of the test section

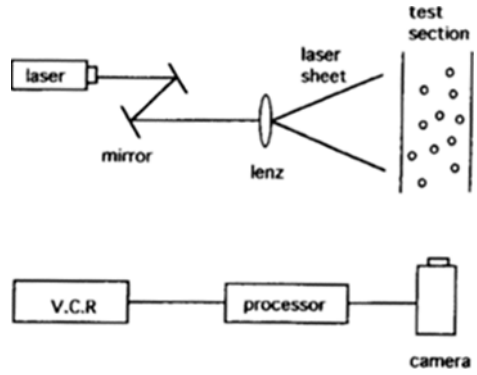


**Fig. 4** Schematic drawing of the flow visualization system

visualized by the laser, and the visualized image was processed using a motion analyzer (Model : EKTAPRO). The laser power was 4 kW. Water or particle velocity was determined from the moving distance and the elapsed time. Moving distance was determined by counting the number of pixels from video image, and the elapsed time was calculated by multiplying the camera exposure rate and the number of video images. Acual length of one pixel was obtained from the image of the glass tube, whose diameter is known precisely.

Experimental uncertainty analysis was conducted. Among the uncertainties, the uncertainty on flow measurement and that on temperature measurement were the major ones, which was 5% and 15% respectively. These yielded the uncertainty on heat transfer coefficient of 16%.

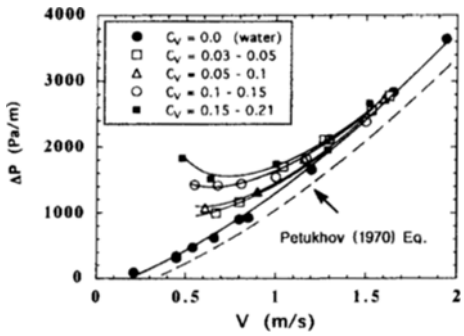


**Fig. 5** Pressure drop data of 3.0 mm glass beads circulating with water

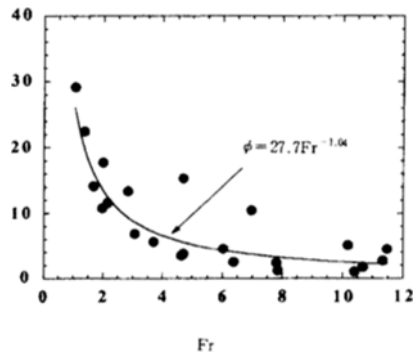


**Fig. 6** Non-dimensional plot of the pressure loss data (3.0 mm glass beads)

## 3. Results and Discussion

### 3.1 Pressure drop test

Flow velocity was determined from the measured flow volume (both water and glass beads), which is the definition of 'superficial velocity'. Pressure drop was measured by a water manometer. For the slurry flow, the density is different from the density of pure water, and the manometer reading should be corrected as follows.

$$\Delta h_p = \Delta h_m - \Delta h_c \quad (1)$$

$$\Delta h_c = C_v (S-1) L \quad (2)$$

Tests were conducted with a known amount of glass beads in the system. Water temperature was maintained at 20°C. During the experiment, however, the particle volume fraction $C_v$ increased as the flow velocity decreased. Figure. 5 shows the pressure loss per unit length plotted against the flow velocity. At flow velocities higher than 1.0 m/s, the pressure loss of the slurry flow becomes independent of the particle volume fraction, and approaches that of the pure water flow. At flow velocities lower than 1.0m/s, however, the slurry flow yields larger pressure loss compared with the pure water flow. The deviation from the pure water increases as the flow velocity decreases and the particle volume fraction increases. Newitt et al. (1961) noticed a similar trend from the sand slurry experiments. The pressure drop data of pure water flow were approximately 15% higher than those predicted by the Petukhov (1970) equation.

The pressure loss data at high particle loading ($C_v$ = 0.15 ~ 0.20) show an inflection point at the flow velocity of approximately 0.6m/s. The occurrence of an inflection point at a low flow velocity is typical of a slurry flow when relatively large particles ($d \geq 50\mu m$) are involved. Detailed information on the hydrodynamics of a slurry flow may be obtained from other sources (Darby, 1986). To understand the pressure loss characteristics of the slurry flow, the particle behavior was investigated through the flow visualization study. The results will discussed in the following sec-

tion.

The pressure loss data may be correlated using a nondimensionalized Froude number.

$$F_r=\frac{V^2C_d^{1/2}}{gD(s-1)} \tag{3}$$

The drag coefficient of a swarm of particles $C_d$ is determined from the following equations (Darby, 1986).

$$C_d=C_{do}/(1+C_v^{1/3}) \tag{4}$$

$$C_{do}=(0.632+4.8\mathrm{Re}_p^{-1/2}) \tag{5}$$

$$Re_p=[(14.42+1.827Ar^{1/2})^{1/2}-3.798]^2 \tag{6}$$

$$Ar=\frac{d^3g(s-1)}{\nu^2} \tag{7}$$

Figure 6 shows the nondimensional pressure loss coefficient $\phi$ plotted against Froude number. Nondimensional pressure loss coefficient $\phi$ is defined as Eq.(8).

$$\phi=\frac{i_m-i_f}{C_vi_f} \tag{8}$$

Figure 6 shows that the present data are reasonably correlated by Eq.(9)

$$\phi=27.7F_r^{-1.04} \tag{9}$$

### 3.2 Heat transfer test

The particles flowing with water periodically hit the tube wall, break the thermal boundary layer, and increase the heat transfer. Particularly when the flow velocity is low, the effect is more pronounced. It is speculated that, as the flow velocity decreases, the hitting frequency may increase, and thus increases the heat transfer. Our flow visualization study showed that this is indeed true. This point will be discussed at the end of the section.

Heat transfer tests were conducted using the same test rig with the heat transfer test section. Heat transfer coefficient 'h' is determined from Eq.(10).

$$h=\frac{Q}{\pi DL(T_w-T_f)} \tag{10}$$

$$Q=(m_wc_{pw}+m_sc_{ps})(T_{out}-T_{in}) \tag{11}$$

Equation(11) assumes that the temperature of water and that of the the glass beads are the same at the same axial location of the test section. The heat transferred to the test section may also be calculated from the voltage and the current supplied. Both calculations agreed with each other within 5%, which confirms that the glass beads are in thermal equilibrium with the water. For the whole experiment, the water inlet temperature $T_{in}$ was maintained at 30℃, and the heat flux to the test section was maintained at 26kW/m$^2$. The water outlet temperature $T_{out}$ changed from 32℃ to 35℃ depending on the flow velocity.

Figure 7 shows the heat transfer coefficient of the slurry flow plotted against the flow velocity. The flow velocity was varied from 0.5m/s to 2.0 m/s, and the particle volume fraction $C_v$ was varied to 0.21. The solid line in the figure denotes the heat transfer coefficient of pure water (McAdams, 1954). Figure 7 shows that, above

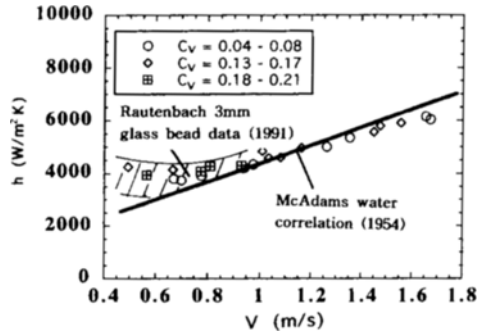


**Fig. 7** Heat transfer coefficient of the slurry flow (3.0 mm glass beads circulating with water)

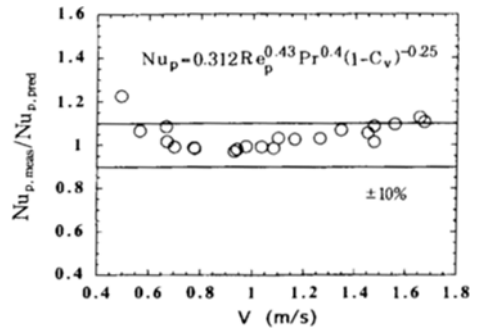


**Fig. 8** Present heat transfer data predicted by the correlation [Eq.(14)]

1.0m/s, the heat transfer coefficient of the slurry flow is approximately the same as that of pure water. Below 1.0 m/s, however, the heat transfer coefficient of the slurry flow is higher. It increases slightly as the particle volume fraction increases, and is almost constant independent of the flow velocity. Rautenbach's(1991) 3.0mm glass bead data are also shown in the figure, which reasonably match with the current data. Regression analysis of the heat transfer data yielded the following correlation.

$$Nu_p = 0.312 Re_p^{0.43} Pr^{0.4} (1 - C_v)^{-0.25} \quad (12)$$

The Prandtl number exponent 0.4 was adopted from the in-tube heat transfer correlation, such as Dittus-Boelter(1930). Figure 8 shows that Eq. (12) correlates the present data within ±10%.

### 3.3 Flow visualization study

Our pressure loss and heat transfer data show that two distinct regimes exist according to the flow velocity. Above the flow velocity 1.0m/s, both the pressure loss and the heat transfer coefficient of the slurry flow approximately match with those of pure water. Below 1.0m/s, the slurry data deviate from those of pure water yielding increased pressure loss and augmented heat transfer. To investigate the mechanism associated with the increased pressure loss and the heat transfer augmentation by particles, flow visualization study was conducted. The apparatus and the data reduction scheme was described in the previous chapter.

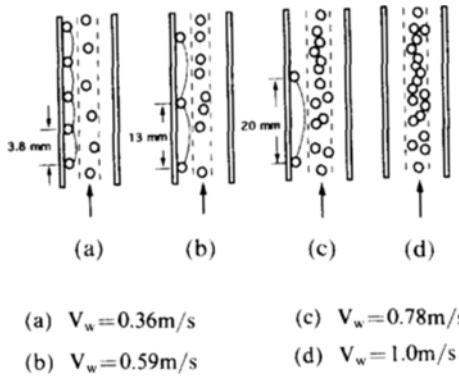


**Fig. 9** Sketch showing particle behavior near tube wall

Figure 9 shows the sketch of the particle behavior near tube wall. Below the flow velocity of 1.0 m/s, particles near the wall moved upward continuously hitting the tube wall. The distance between the hitting to the next hitting increased as the flow velocity increased. At the water flow velocity of 0.36m/s, the average distance was 3.8 mm. At 0.59m/s, it increased to approximately 13 mm, and to 20mm at 0.78m/s. Above 1.0m/s, no hitting was observed. Our experimental data show an increased pressure loss and augmented heat transfer at the flow velocities lower than 1.0m/s. This may be explained qualitatively as follows. The particles hitting the tube wall exchange hydrodynamic momentum with the wall as well as they break the thermal boundary layer, which yields the increased pressure loss and heat transfer. Figure 9 also shows that, above the flow velocity of 1.0m/s, all the particles move toward the center of the tube leaving an annulus of clear water near the wall. This may be the reason why the slurry flow shows approximately equal pressure loss and heat transfer coefficient to those of pure water flow at the flow velocities higher than 1.0m/s.

It was also observed that particles near the wall were not entrained to the main flow. They continuously hit the wall remaining within a horizontal distance of approximately 4 mm from the wall. Tube inner diameter was 12mm. The particles located at the central portion of the tube did not move toward the wall. They remained at the central portion. Currently, no adequate explanation may be provided why particles do not mix. If a particle is situated near the tube wall where the velocity gradient is steep, it will be subjected to forces which tend to cause it rotate and to move towards the center of the tube. This phenomenon is called 'Magnus effect'. The magnitude of the force increases as the flow velocity increases. This may explain why more particles flow at the central portion at a higher flow velocity.

Figure 10 shows the particle slip velocity plotted against the water velocity. Figure 10 shows that the slip velocity is largest(0.37m/s) at the

water velocity of 0.55m/s. Large slip velocity implies small flow resistance. Pressure drop data in Fig. 4 indeed show a minimum(for $C_v$= 0.15−0.20) near the flow velocity of approximately 0.6m/s. The particle Reynolds number associated with this slip velocty was 1110.

### 3.4 Fouling test

Main advantage of a liquid fluidized bed heat exchanger is the prevention of fouling. Fouling tests were conducted at the heat transfer loop. To accelerate fouling, 30,000ppm of ferric oxide($Fe_2O_3$) was added to the flowing medium. Ferric oxide was chosen because it is one of the main component of a common fouling deposit. The ferric oxide used in this study has a mean particle diameter 0.98$\mu$m and a specific gravity of 5.12.

Fouling tests initiated by pouring an adequate amount of ferric oxide into the circulating water after the system was thermally stabilized. As time elapsed, the ferric oxide deposited at the tube wall yielding heat transfer degradation. The fouling curve is shown in Figure 11. During the test, the flow velocity was maintaind at 0.8 m/s. The particle volume fraction was 0.1. Experiments were conducted in two different ways - one with glass beads from the start(shown as a open symbol in the figure), the other glass beads added after sufficient fouling occurred(shown as dark symbol). Figure 11 shows that the heat transfer coefficient maintained the initial value when the glass beads were circulated from the start. The glass beads are thought to prevent the ferric oxide deposit buildup by continuously hitting the tube wall. When the foulant-water mixture was circulated without glass beads, the heat transfer coefficient rapidly decreased. The fouling curve shows an asymptotic shape, which is typical in particulate fouling. The glass beads were added after 65 hours of operation, when the heat transfer coefficient decreased to one third of the initial value. The heat transfer coefficient increased immediately, and approached to that of the clean slurry flow. All these reveal that particles effectively remove the pre-exsisting deposit as well as they prevent deposit buildup.

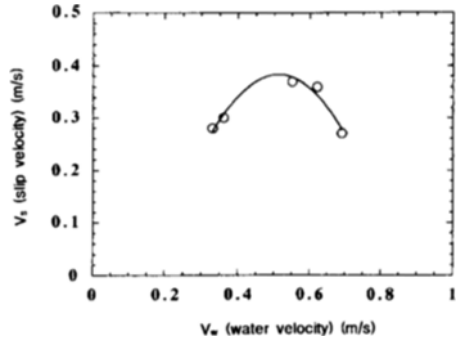


**Fig. 10** Slip velocity of a particle plotted against water velocity

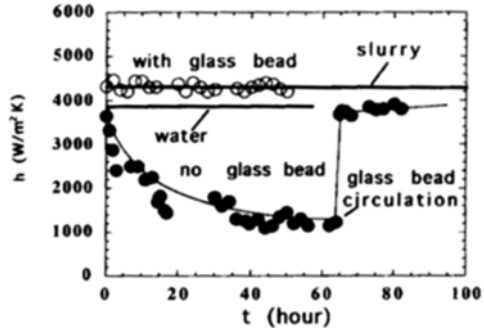


**Fig. 11** Fouling curves obtained when 30000ppm of $Fe_2O_3$ circulating in water at V=0.8m/s and $C_v$=0.1

## 4. Conclusions

In this study, the pressure loss, the heat transfer coefficient and the fouling characteristics of the slurry flow were investigated. The particles used were the glass beads of 3.0 mm diameter with 2.54 specific gravity. Listed below are main findings.

(1) The particles augmented the heat transfer at the flow velocities lower than 1.0m/s. In this range, the heat transfer coefficient slighly increased as the particle volume fraction increased, and was almost independent of the flow velocity.

(2) The pressure loss also exceeded that of pure water at the flow velocities lower than 1.0 m/s. In

this range, the pressure loss increased as the particle volume fraction increased.

(3) From the observation of the particle behavior near tube wall, the heat transfer and the pressure loss characteristics are believed to be closely related with the tube wall collision frequency of the flowing particles.

(4) The particles effectively controlled fouling. Fouling tests using ferric oxide revealed that the particles effectively removed the pre exsisting deposit as well as they prevented the deposit buildup.

(5) The present pressure loss data are correlated to Eq.(9), and the heat transfer data are correlated to Eq.(12).

## Acknowledgment

This research was funded from Korean Government through G-7 project.

## References

Darby, R., 1986, *Encyclopedia of Fluid Mechanics*, Gulf Publishing Co., Vol. 5-1, pp. 49~91.

Dittus, F. W. and Boelter, L. M. K., 1930, Univ. Calif., Berkeley, *Publ. Eng.*, Vol. 2.

Klaren, D. G., 1983, "The Fluidized Bed Heat Exchanger: Principles and Modes of Operation and Heat Transfer Results under Severe Fouling Conditions," *Fouling Prev. Res. Dig.*, Vol. 5, No. 1.

Hatch, L. P. and Weth, G. G., 1970, "Scale Control in High Temperature Distillation Utilizing Fluidized Bed Heat Exchangers," *R &D Progress Report*, No. 571.

McAdams, W. H., 1954, *Heat Transmission*, McGraw-Hill Co.

Newitt, D. M., Richardson, J. F. and Gliddon, B. J., 1961, "Hydraulic Conveying of Solids in Vertical Pipes," *Trans. Instn. Chem. Engrs.*, Vol. 39, pp. 93~100.

Petukhov, B. S., 1970, "Heat Transfer in Turbulent Pipe Flow with Variable Physical Properties," in *Advances in Heat Transfer*, Vol. 6, T. F. Irvine and J. P. Hartnett, Eds., Academic Press, New York, pp. 504~564.

Rautenbach, R., Erdmann, C. and Kolbach, J. St., 1991, "The Fluidized Bed Technique in the Evaporation of Wastewater with Severe Fouling/Scaling Potential -Latest Developments, Applications, Limitations," *Desalination*, Vol. 81, pp. 285~298